Hindawi
Geofluids
Volume 2021, Article ID 9373948, 17 pages
https://doi.org/10.1155/2021/9373948

Research Article

Reservoir Characteristics of the Lower Permian Marine-Continental Transitional Shales: Example from the Shanxi Formation and Taiyuan Formation in the Ordos Basin

H. Wang,[1,2,3] **L. Zhang**,[1,2,3] **Q. Zhao**,[1,2,3] **Z. Qiu**,[1,2,3] **D. Liu**,[1,2,3] **Q. Zhang**,[1,2,3] **Y. Wang**,[1,2,3] **and D. Dong**[1,2,3]

[1]*Research Institute of Petroleum Exploration and Development, China National Petroleum Corporation (CNPC), Beijing 100083, China*
[2]*National Energy Shale Gas Research & Development (Experiment) Center, Langfang 065007, China*
[3]*CNPC Key Laboratory of Unconventional Oil and Gas, Langfang 065007, China*

Correspondence should be addressed to L. Zhang; 137910299@qq.com

Received 2 September 2021; Accepted 7 November 2021; Published 7 December 2021

Academic Editor: Chao Liang

The pore types and pore structure parameters of the heterogenetic shale will affect the percolation and reservoir properties of shale; therefore, the research on these parameters is very important for shale reservoir evaluation. We used X-ray diffraction (XRD) analysis, scanning electron microscopy (SEM), low-pressure CO_2 adsorption analysis, mercury injection capillary pressure (MICP), and high-pressure methane adsorption analysis to analyze the characteristics of different pore types and their parameters of the Lower Permian Shanxi Formation and Taiyuan Formation in the Ordos Basin. The influence of different mineral contents on the porosity and pore size is also investigated. The Shanxi Formation (SF) is composed of quartz (average of 38.4%), plagioclase, siderite, Fe-dolomite, calcite, pyrite, and clay minerals (average of 50.1%), while the Taiyuan Formation (TF) is composed of calcite (average of 37%), siderite, Fe-dolomite, quartz, pyrite, and clay minerals (average of 32.3%). The most common types of pores observed in this formation are interparticle pores (InterP pores), intraparticle pores (IntraP pores), interclay pores, intercrystalline pores (InterC pores), organic matter pores (OM pores), and microfractures. CO_2 adsorption analysis demonstrates the type I physisorption isotherms, showing microporous solids having comparatively small external surfaces. The similar types of isothermal shapes of the Shanxi Formation (SF) and Taiyuan Formation (TF) suggest that both types have similar pore size distribution (PSD) within the measured pore range by the low-pressure CO_2 adsorption experiment. The micropore pore size of the TF is larger than that of the SF. MICP shows the larger pores (>50 nm), and most of the volume was adsorbed by macropores. Methane gas sorption capacity increases with increasing pressure. Clay minerals and quartz played an important role in providing adsorption sites for methane gas. The overall analysis of both formations shows that TF has good reservoir properties than SF.

1. Introduction

One of the most important types of unconventional hydrocarbon resources is shale gas resources that play a vital role in fulfilling the global energy demand. Due to extensive drilling, conventional oil and gas resources are becoming scarcer. This scarcity boosts the discovery and usage of unconventional oil and gas resources globally [1, 2]. Recently, shale oil and gas resources are the main exploration targets that succeeded the conventional oil and gas resources [3–6]. China has humongous shale gas resources distributed in various basins, i.e., Sichuan Basin, Ordos Basin, and Junggar Basin [3, 7, 8], and many other basins that have very broad prospects. The vertical heterogenic behavior of shale reservoirs has been extensively studied, and it was found that paleoredox conditions, sea-level fluctuations, and biogenic productivity contributed directly to the vertical heterogeneity of shale [9–14].

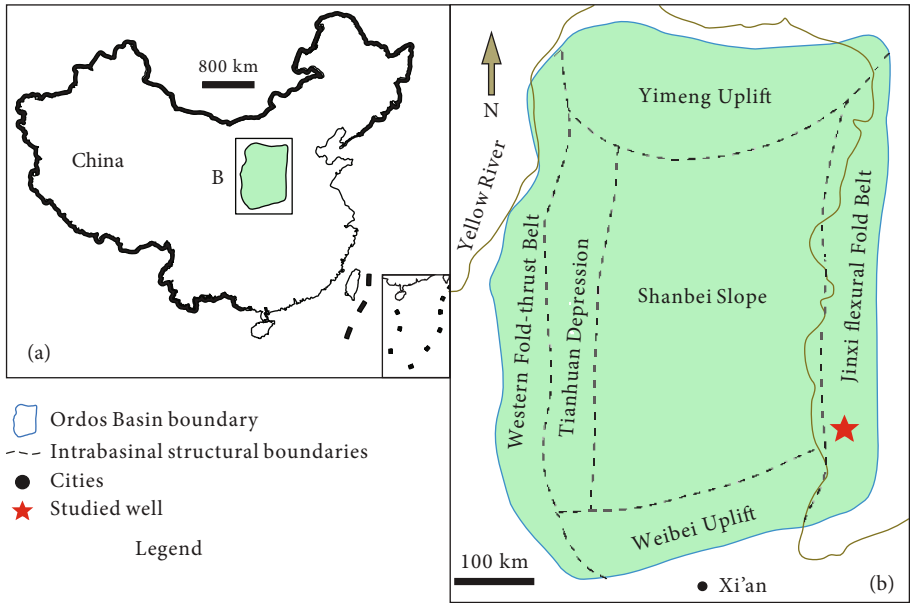

Figure 1: Location map of the study area in the Ordos Basin. The star shows the position of a well (DJ3-4) in the study area (modified after [46]).

The reservoir properties and storage mechanism in the shale are quite different and complex than conventional reservoirs; it may contain a free compressed gas, dissolved gas, and adsorbed gas [15–21]. After the successful horizontal drilling and hydrofracking, shale gas reservoirs gain huge attention. Different types of pores within the shale gas reservoirs are micro- to nanoscale in size with random distribution [22, 23]. The effective evaluation of shale gas reservoirs is quite difficult because of their higher level of heterogeneity. The shale gas reservoirs can be characterized and evaluated comprehensively with the help of lithofacies analysis that is directly correlated to the mineralogical composition, geochemistry, petrology, and petrophysical parameters of rocks [24]. Different lithofacies have different pore types, and each pore type has diverse physiochemical properties (structure and pore surface properties) that cause significant variations in the reservoir properties of shale.

The marine-continental transitional shales of the Lower Permian Shanxi Formation and Taiyuan Formation in the Ordos Basin are characterized by thick sequence, moderate maturity, high TOC content, and good gas potential [25, 26]. The depositional settings of the Carboniferous to Permian shales have been studied in detail in the Ordos Basin [27–29]. Previous research shows that the reservoir parameters have a huge impact on hydrocarbon reserves [30–32]. PSD and throat distribution and their potential connectivity vary with diverse geological environmental conditions [33]. The Shanxi Formation and Taiyuan Formation are the important shale gas places in the Ordos Basin. However, to date, very few detailed studies have been conducted to characterize the reservoir physiognomies of the Lower Permian Shanxi Formation and Taiyuan Formation in the Ordos Basin [34–36]. In this manuscript, the Lower Permian Shanxi Formation and Taiyuan Formation from the DJ3-4 were sampled and studied employing a detailed analysis of whole-rock mineral composition (XRD analysis), SEM petrographic analysis, high-pressure methane adsorption analysis, low-pressure CO_2 adsorption analysis, and high-pressure mercury injection (MICP) analysis to characterize and evaluate the reservoir parameters of the Lower Permian Shanxi Formation and Taiyuan Formation in the Ordos Basin.

2. Geological Background

The Ordos Basin is the rectangular-shaped sedimentary craton basin having an area of 370,000 square kilometers, located in the west part of the North China Platform [37–39]. This basin has undergone four tectonic evolutionary stages: (i) the Lower Paleozoic shallow marine platform, (ii) the Upper Paleozoic offshore basin, (iii) the Mesozoic intracontinental basin, and (iv) the Cenozoic faulting and subsidence, and it was mainly developed during the Mesozoic period [40]. The Ordos Basin can further be divided into six different units (Yimeng Uplift, Western Fold and Thrust Belt, Tianhuan Depression, Shanbei Slope, Jinxi Flexural Fold Belt, and Weibei Uplift) [41, 42] (Figure 1). A thick sequence of carbonate rocks was deposited in the marine settings from Proterozoic-Lower Paleozoic time [25, 43]. The Carboniferous to Permian system is a distinctive marine-continental transitional system that results in the deposition of interbedded shale, sandstones, coal, and carbonate rocks in the Upper Carboniferous Benxi Formation, the Lower Permian Taiyuan Formation, and the Shanxi Formation in the Ordos Basin [44–46] (Figure 2). The well DJ3-4 is located in the southeast part of the Ordos Basin.

3. Data and Methodology

3.1. X-Ray Diffraction Analysis. The whole-rock mineral composition has been identified by using XRD analysis.

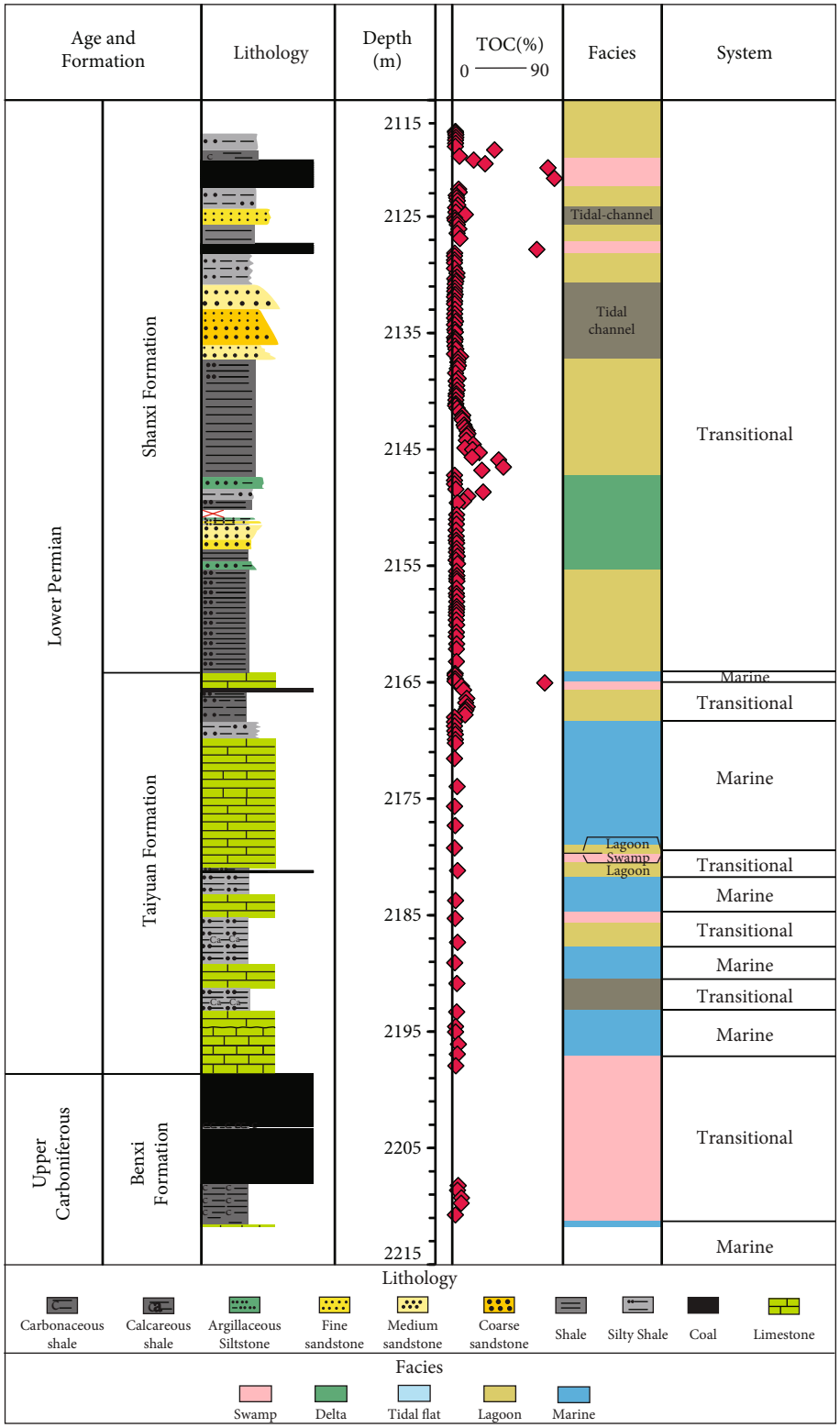

FIGURE 2: Stratigraphic chart of the study area. The Lower Permian Shanxi and Taiyuan formations are investigated in this study (modified from [46]).

Samples of the Shanxi Formation and Taiyuan Formation from the Ordos Basin were analyzed for whole-rock mineral and whole-rock clay fraction composition using the PANalytical X'Pert Pro X-ray Diffractometer equipped with a copper X-ray source (Co-Kα radiation, 40 kV, 40 mA). Each sample weighing 5 g was dried for two days in an oven, then

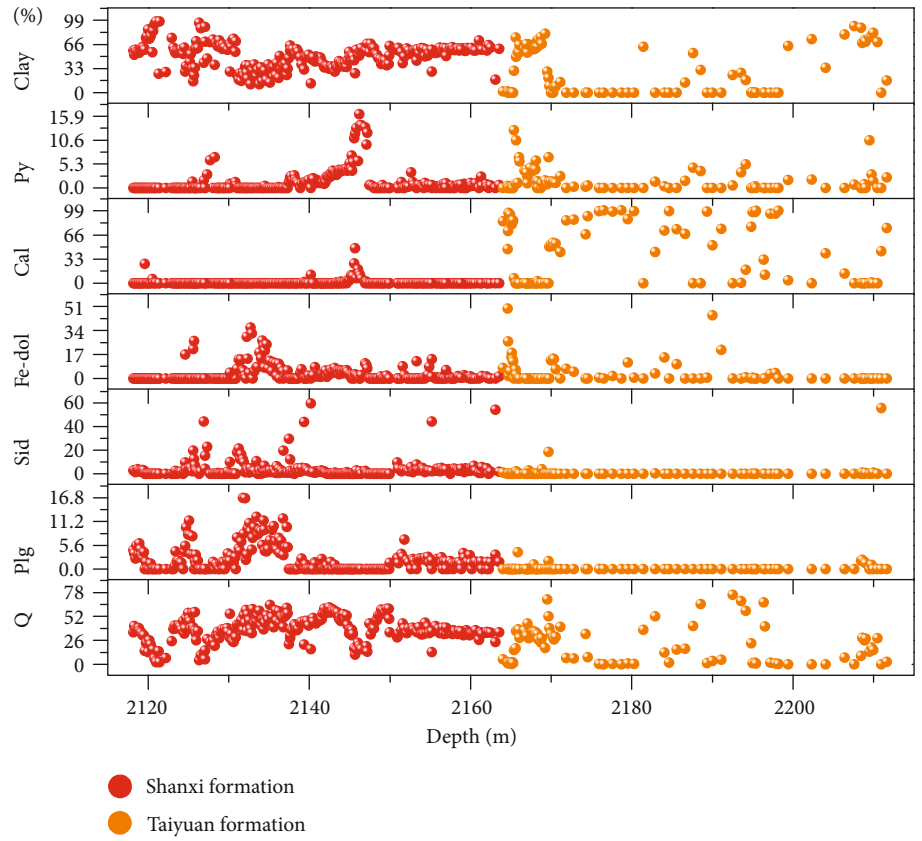

Figure 3: Showing the vertical distribution of various minerals in the Shanxi Formation and Taiyuan Formation in the Ordos Basin. Note: Q = quartz; Plg = plagioclase; Sid = siderite; Py = pyrite; Cal = calcite; Fe-dol = Fe-dolomite.

Table 1: Mineralogical composition of representative samples of the Shanxi Formation and Taiyuan Formation in the Ordos Basin.

Formation	Quantity	Quartz (%)	Plagioclase (%)	Siderite (%)	Fe-dolomite (%)	Calcite (%)	Pyrite (%)	Clay (%)
Shanxi	Min	2.3	0	0	0	0	0	11.6
	Max	64.3	16.8	59.7	36.3	47.7	16.3	97.7
	Avg	38.5	2.2	3.7	3.0	1.1	1.3	50.1
Taiyuan	Min	0	0	0	0	0	0	0
	Max	75.5	4.0	56.0	49.7	100	12.8	91.3
	Avg	22.3	0.2	1.8	4.1	37.2	1.7	32.7

ground to powder form having <200 mesh size with agate mortar and pestle. The angle range was 5-10° at the rate of 2θ for the whole-rock mineral and clay fraction analysis.

3.2. Scanning Electron Microscopy. Based on the mineralogical composition, shale samples from Shanxi and Taiyuan formations having diverse mineralogy were selected for scanning electron microscopy (SEM) to investigate the contrasting features of various minerals and distribution of micro-nanopores, microfractures, and organic matter (OM). Shale samples from these two formations were selected for SEM analysis. For SEM analysis, shale samples were first polished with argon ions to increase their smoothness and then coated with Au to enhance their electrical conductivity. This analysis was performed on a LEO SEM (Model: LEO1450VP) coupled with EDS (Energy-Dispersive Spectroscopy).

3.3. CO_2 Adsorption Analysis. The pore structure composed of the pore size distribution (PSD), pore volume, and specific surface area (SSA) of shale was studied by low-pressure gas adsorption analysis (less than 18.4 psi). The required samples having 60-100 mesh sizes were degassed for 18 hours to clean the pore surface. This experiment was carried out using the QUADRASORB Station 1 apparatus. Low-pressure CO_2 gas adsorption (LP-CO_2-GA) was conducted at 273.15 K temperature to demonstrate the micropores (ranging from 0.35 nm to 2 nm). The micropores (<2 nm) were calculated by using the Density Functional Theory

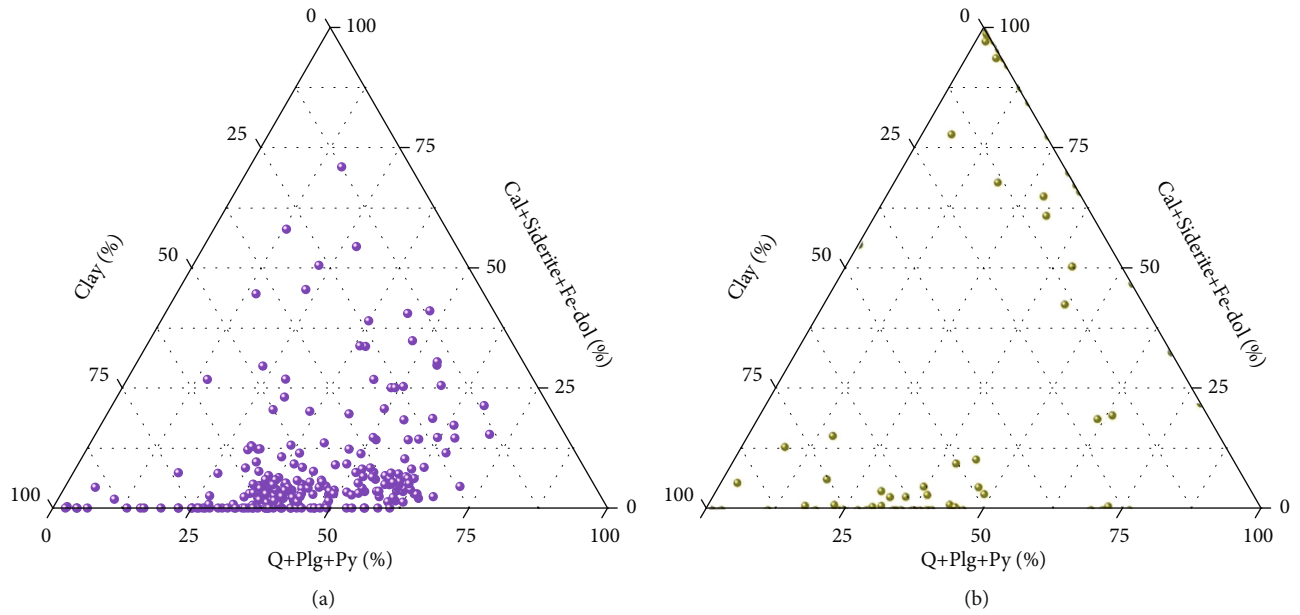

Figure 4: (a) Ternary diagram showing the distribution of different minerals in the Shanxi Formation. (b) Ternary diagram showing the distribution of different minerals in the Taiyuan Formation. Note: Q = quartz; Plg = plagioclase; Py = pyrite; Cal = calcite; Fe-dol = Fe-dolomite.

(DFT) model [47]. The characteristics of isotherms were interpreted using predefined patterns by Sing et al. [48].

3.4. Mercury Injection Capillary Pressure Analysis. MICP analysis was carried to measure the pore size of macropores (>50 nm) in the Lower Permian shale by using the Mercury Intrusion Porosimeter of the Quantachrome PoreMaster 60. The shale rock piece from each sample was desiccated in a vacuum oven for 24 hours at 423 K, and then approximately 1.53 g of each sample was loaded into a penetrometer to obtain the pressure and volume of mercury intrusion and extrusion. Mercury (nonwetting fluid) is used to enter the pores by ensuing these parameters: mercury density of 13.53 g/mL, Hg surface tension as 480 erg/cm, and contact angle of 140°. Mercury filling pressure of 0.51 psi was applied, followed by injecting high pressure (0.1 MPa-413.7 MPa equals 60,000 psi) related to the pore throat size (3.6 nm-1100 μm). The pore throat distribution was probed in this research work by using the Washburn equation (1) in the case of cylindrical pores [49].

$$r_i = \frac{-2\sigma \cos\theta}{P_c}, \tag{1}$$

where r_i is the pore throat radius calculated in μm, σ is the surface tension of Hg (480 erg/cm), θ is the contact angle of Hg (140°), and P_c is the mercury injection pressure (ranging from 14.5 psi to 60,000 psi).

3.5. High-Pressure Methane Adsorption Analysis. The methane adsorption isotherms (20-100°C; up to 12 MPa) were performed on the FY-KT 1000 isothermal adsorption device under equilibrium moisture settings adopting Chinese National Standard Testing (GB/T 19560-2004) at the Research Institute of Petroleum Exploration and Development, Langfang, China. The representative shale samples having 104.25 g mass were ground and sieved to <60 mesh size (less than 250 microns) particles. We achieved equilibrium moisture conditions under controlled relative humidity (RH) conditions in an evacuated desiccator through saturated salt conditions of K_2SO_4 (RH = 97%). To achieve the constant weight, the samples were weighed once after every 24 hours, and the process continued for three days. The detailed information regarding this experiment was extensively described by Ji et al. [50]. The experimental methane adsorption data from shale samples were parameterized using the Langmuir sorption model [51]:

$$V = \frac{V_L P}{P_L + P}, \tag{2}$$

where "V" is the gas sorption volume per unit weight of the shale sample (cm^3/g rock) in equilibrium at a certain pressure, "V_L" in the Langmuir volume based on monolayer adsorption which represents the maximum adsorption capacity of gas at complete surface exposure, "P" is the gas pressure (MPa), and "P_L" represents the Langmuir pressure (MPa) at which the total adsorbed volume is equal to one-half of the Langmuir volume.

4. Results and Discussion

4.1. Mineralogical Composition of the Shale Samples. The Shanxi Formation and Taiyuan Formation have diverse mineralogical compositions. XRD analysis shows that the Shanxi Formation (SF) is composed of quartz (average of 38.4%), plagioclase (average of 2.24%), siderite (average of 3.70%), Fe-dolomite (average of 3%), calcite (average

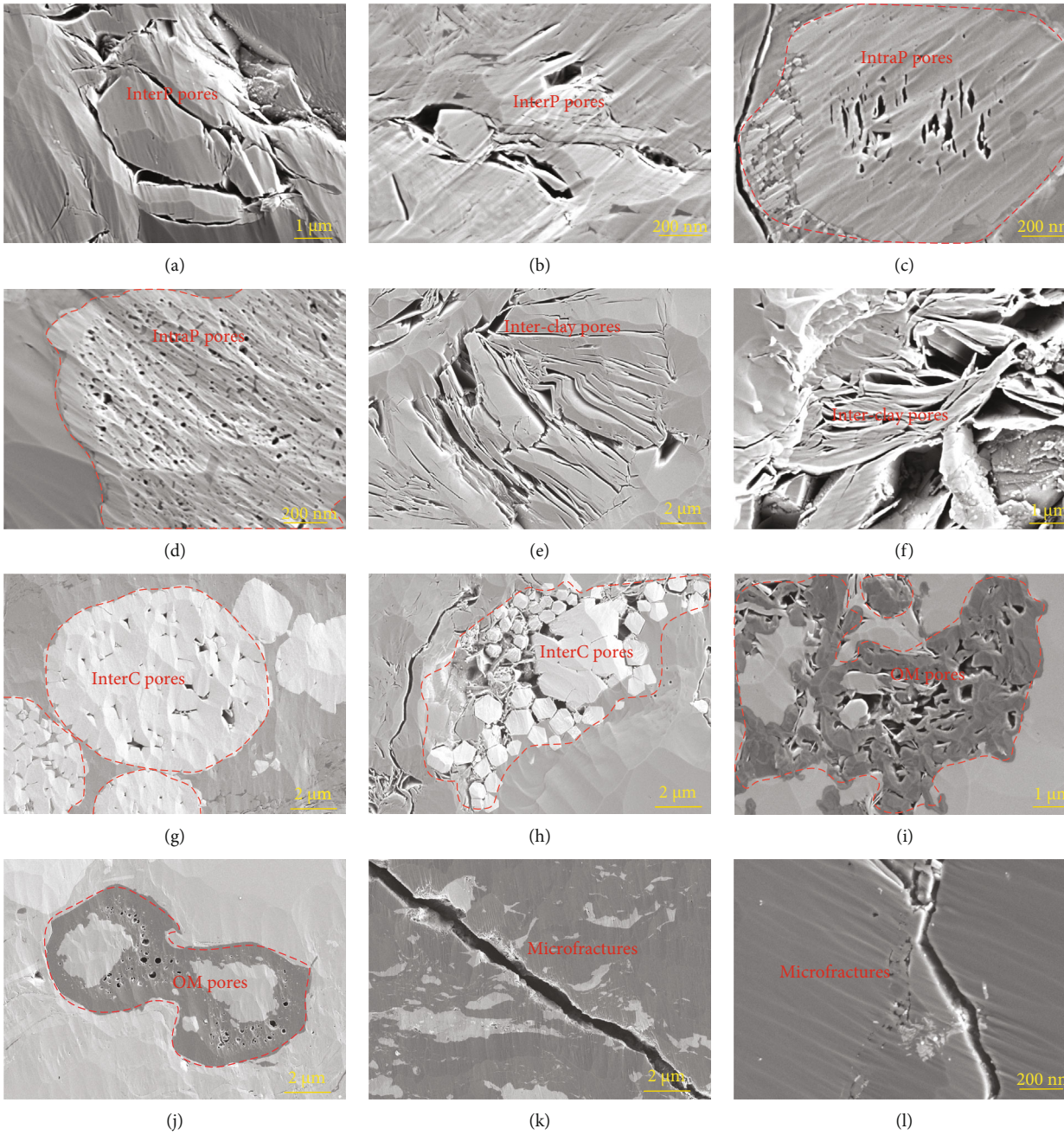

Figure 5: The presence of different pore types in the Shanxi Formation and Taiyuan Formation. (a, b) InterP pores, 2118.93 m, 2122.22 m. (c, d) IntraP pores, 2129.20 m, 2120.31 m. (e, f) Interclay pores, 2125.10 m, 2151.41 m. (g, h) InterC pores, 2135.98 m, 2145.29 m. (i, j) OM pores, 2143.59 m, 2134.16 m. (k, l) Microfractures, 3136.56 m, 2137.66 m.

of 1%), pyrite (average of 1.29%), and clay minerals (average of 50.1%) (Figure 3, Table 1), while the Taiyuan Formation (TF) is composed of calcite (average of 37%), siderite (average of 1.24%), Fe-dolomite (average of 3.69%), quartz (average of 21.9%), pyrite (average of 1.59%), and clay minerals (average of 32.3%) (Figure 3, Table 1). The ternary diagrams display the diversity of the whole-rock mineral compositions of the Lower Permian Shanxi Formation and Taiyuan Formation in the Ordos Basin (Figures 4(a) and 4(b)).

4.2. Pore Types and Pore Size Distributions of the Shanxi Formation and Taiyuan Formation

4.2.1. Characteristics of Different Pore Types via SEM. There are various types of pores encountered in the Shanxi Formation and Taiyuan Formation in the Ordos Basin via SEM analysis. We divided the pores according to Loucks et al. [23], i.e., interparticle (InterP) pores, intraparticle (IntraP) pores, interclay pores, intercrystalline (InterC) pores, organic matter (OM) pores, and microfractures.

Table 2: Average pore size, pore volume, and pore surface area of the micropores in the SF and TF by CO_2 adsorption analysis and average pore diameter, throat/pore ratio, total pore volume, and total pore surface area of the meso-macropores in the Shanxi Formation and Taiyuan Formation by MICP analysis.

Formation	Depth (m)	CO_2 adsorption			MICP analysis			
		Average pore size (nm)	S_{DFT} (m^2/g)	V_{DFT} (10^{-3} cc/g)	Average pore diameter (nm)	Throat/pore ratio	Total volume (10^{-3} cc/g)	Total surface area (m^2/g)
Shanxi	2145.86	0.853	35.575	11.00	504	0.2437	1.20	0.3447
	2146.23	0.829	36.032	10.00	513	0.2394	1.30	0.3598
	2146.48	0.848	87.67	26.00	520.5	0.7308	5.00	1.3204
	2147.11	0.857	108.74	33.00	520.7	0.7037	10.30	2.7035
	2147.49	0.848	107.64	32.00	567.7	0.7225	7.00	1.4798
	2147.9	0.85	138.3	41.00	567.7	0.7225	11.70	2.9467
	2148.28	0.86	100.25	30.00	747.1	0.8547	7.10	1.8181
Taiyuan	2164.31	0.65	2.585	1.00	600.09	0.9845	0.30	0.0737
	2165.61	0.846	2.476	1.00	600.09	3.1854	2.80	0.4109
	2165.87	0.647	3.746	1.00	477.9	1.2472	1.00	0.3076
	2166.09	0.733	9.479	3.00	477.9	0.9882	0.70	0.1323
	2166.95	0.854	37.473	11.00	504.2	1.2212	0.50	0.1139
	2167.23	0.616	5.241	1.00	504.2	0.0007	1.20	0.3966
	2167.69	0.845	18.524	6.00	480.3	0.0927	0.80	0.0078
	2168.04	0.848	38.803	11.00	480.3	1.0052	1.70	0.2795
	2168.26	0.851	40.892	12.00	548.7	0.9888	0.50	0.2271
	2168.41	0.859	40.472	12.00	548.7	0.9888	0.60	0.1669

InterP pores are mostly encountered in feldspars, quartz, clay floccules, and pyrite framboids and are also present at the edges of particles that are exposed to stress. The shape of the InterP pores is triangular, polygonal, and irregular with nm scale. InterP pores contribute to improving the reservoir quality of the shale and are mostly encountered in brittle minerals that also help to enhance the fracture potential of the shale during reservoir development. In our study area, these pores decrease in concentration with increasing burial depth but some of them may preserve between compacted grains (Figures 5(a) and 5(b)).

IntraP pores are mostly observed within the feldspar, calcite, and dolomite grains (Figures 5(c) and 5(d)). The shape of the IntraP pores is linear, elliptical, and irregular while they are in nm size. These pores are the product of the diagenesis of various minerals and contribute to improving the reservoir properties of the Shanxi Formation and Taiyuan Formation in the Ordos Basin.

Interclay pores are mostly encountered between clay particles. The shape of these pores is triangular and slit-like while their size ranges from nm to mm. These pores also play a vital role in improving the reservoir porosity of the shale (Figures 5(e) and 5(f)).

InterC pores are mostly detected among the crystal of pyrite within the framboidal structure and clay minerals and observed in irregular or small spherical shapes. The size of these pores varies from nm to μm. InterC pores are abundantly distributed in the pyrite framboids and help to store the gas molecules significantly in the Shanxi Formation and Taiyuan Formation in the Ordos Basin (Figures 5(g) and 5(h)).

OM pores are mostly distributed in organic matter and observed in irregular, small spherical, or slit shapes (Figures 5(i) and 5(j)). These types of pores are developed due to the hydrocarbon generation in the organic matter [23]. OM pores are developed in the Shanxi Formation and Taiyuan Formation, especially in OM-rich intervals. They mainly occur as nm size, but their contributions for gas storage in shale are very important.

Microfractures in this shale are developed due to three possible reasons: (i) tectonic activities, (ii) shrinkage of minerals during the diagenetic process, and (iii) overpressure during hydrocarbon generation and expulsion. The microfractures readily occur around the rigid particles and in the organic matter in the SF and TF (Figures 5(k) and 5(l)). These microfractures enhance the reservoir porosity and also provide a migration pathway in shale gas systems [28].

4.2.2. Characteristics of Micropores by the CO_2 Adsorption Technique. Low-pressure CO_2 adsorption analysis was applied to characterize and investigate the pores having <2 nm (micropores) in size in the Lower Permian Shanxi Formation and Taiyuan Formation. The averages of pore size, DFT specific surface area, and DFT volume of the Shanxi Formation and Taiyuan Formation shales are shown in Table 2. The CO_2 adsorption isotherms of both types of shales (SF and TF) of the Shanxi and Taiyuan formations, as shown in Figure 6(a), do not show plateaus and can be categorized as type I physisorption isotherms [48], showing microporous solids having comparatively small external surfaces. The similar types of isothermal shapes of the SF and TF suggest that both types have similar pore size distribution

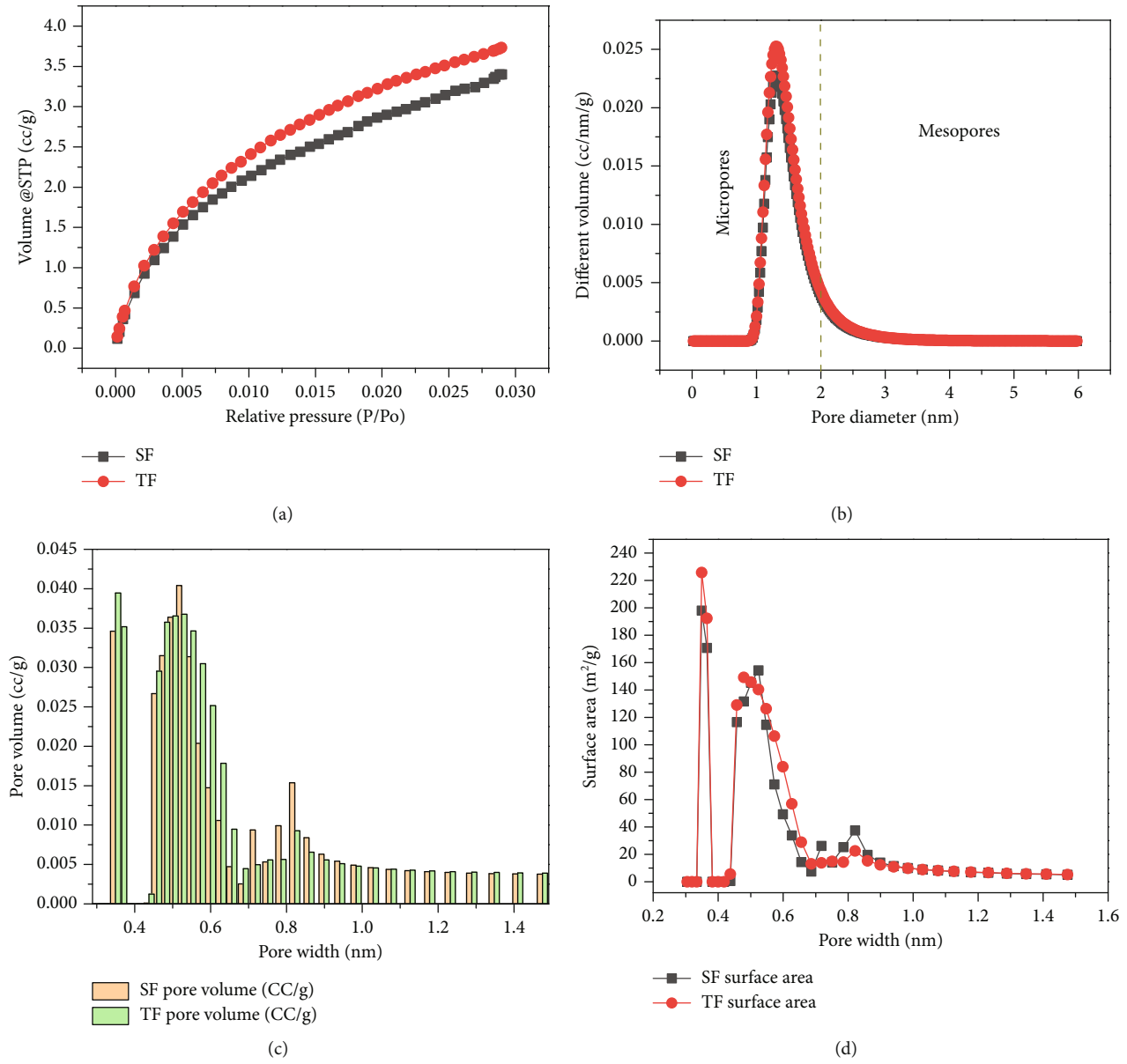

FIGURE 6: The description of micropore parameters in the Shanxi Formation and Taiyuan Formation in the Ordos Basin. (a) CO_2 adsorption isothermal curves. (b) Micropore distribution in the SF and TF. (c, d) Micropore volume and surface area in the Shanxi Formation and Taiyuan Formation.

(PSD) within the measured pore range by the low-pressure CO_2 adsorption experiment.

PSDs of the micropores using the DFT model of the SF and TF samples are shown in Figure 6(b). The pores are mostly scattered in the zone less than 2 nm for both shales (Figure 6(b)). PSDs are mostly characterized by three volumetric maxima (at pore diameters of about 0.36 nm, 0.56 nm, and 0.81 nm) within the pore size range of less than 1 nm. Over 50% of the total micropore volume is principally contributed by the pore diameter between 0.43 nm and 0.81 nm. The pore size > 0.83 nm shows the little pore volume (Figure 6(c)). The specific surface area of the TF is higher than that of the SF, and most of the surface area in both types of shales is provided by the pore size between 0.35 nm and 0.6 nm (Figure 6(d)).

The correlation between the different minerals and the DFT pore volume of the micropores is shown in plot diagrams. The correlation between quartz and DFT pore volume of the micropores is weakly positive (Figure 7(a)), and this relation suggests that the quartz mineral has a very low contribution to the micropore volume. The correlation between calcite and DFT pore volume of the micropores shows a negative relationship (Figure 7(b)), suggesting that the calcite has no contribution to the micropore volume. The clay minerals also show a very weak positive relationship with the DFT pore volume of the micropores

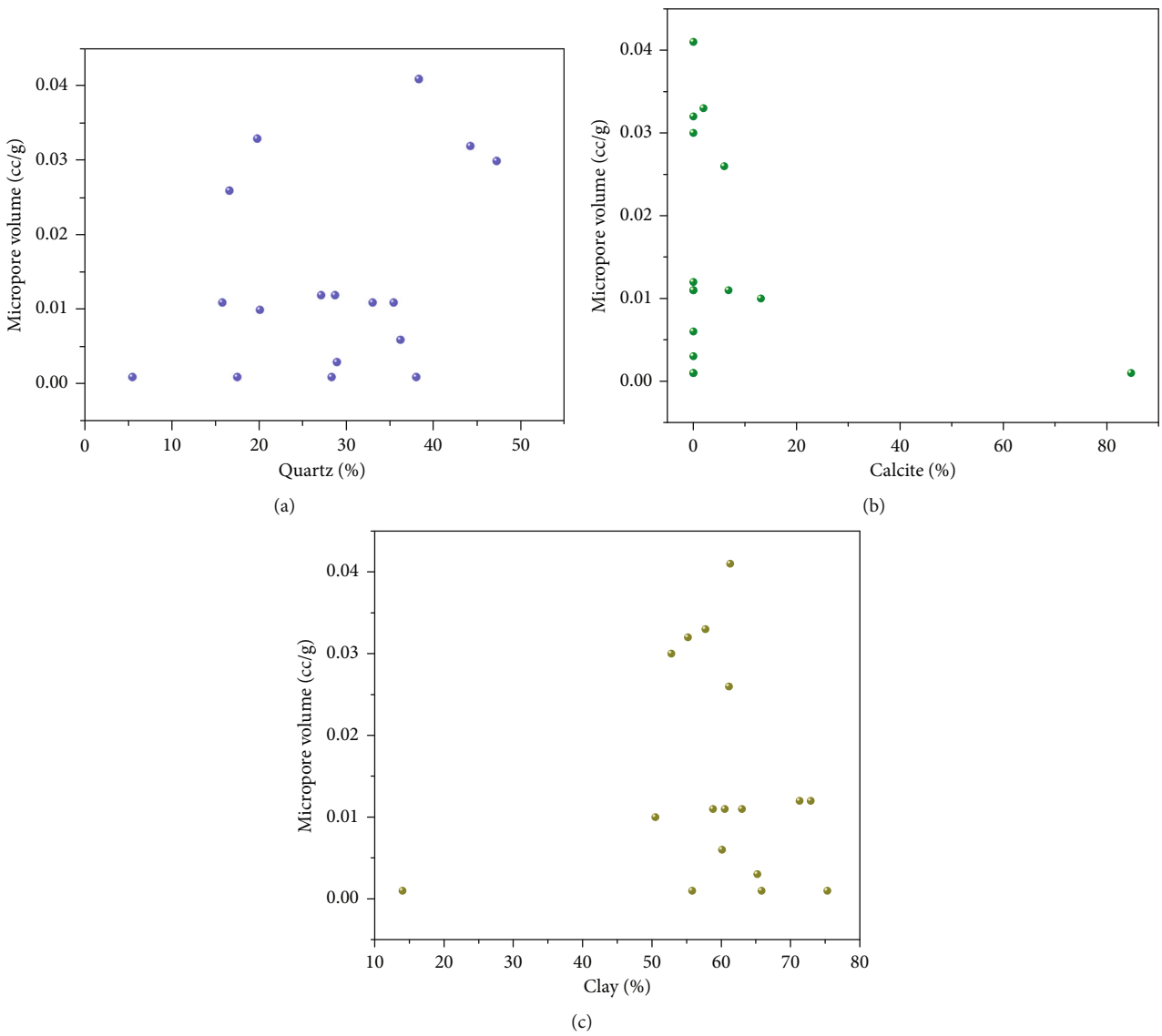

Figure 7: The correlation of micropore volume with different minerals of the Shanxi Formation and Taiyuan Formation, Ordos Basin. (a) Correlation between quartz and micropore volume. (b) Correlation between calcite and micropore volume. (c) Correlation between clay minerals and micropore volume.

(Figure 7(c)), which shows that clay also did not play a good role in micropore volume contribution. Overall, minerals did not show a strong contribution to the micropore volume. So, here, we can propose that the TOC and diagenetic events can have a good contribution to the micropore volume, but to prove that proposal, we need TOC analysis to confirm it.

4.2.3. Mesopore and Macropore Parameters through MICP Analysis. The MICP method directly measures pressure and volume using injected mercury volume. The average pore diameter, throat/pore ratio, total volume, and total surface area determined by MICP analysis are shown in Table 2. The average pore diameter of the meso-macropores of both the Shanxi Formation and the Taiyuan Formation is 562.96 nm and 522.24 nm, respectively. The average throat/pore ratio of the Shanxi Formation and Taiyuan Formation is 0.60 and 1.07, respectively. The average total volume and total surface area of the Shanxi Formation are 0.006 cc/g and 1.57 m^2/g, respectively, while the average total volume and total surface area of the Taiyuan Formation are 0.001 ccc/g and 0.22 m^2/g, respectively.

Figures 8(a) and 8(b) represent the mercury intrusion and extrusion curves for the Shanxi Formation while Figures 8(c) and 8(d) show the mercury intrusion and extrusion curves for the Taiyuan Formation. The MICP curves in both types of formations (Shanxi Formation and Taiyuan Formation) show the distribution of mesopores and macropores in the study, but the concentration of macropores is high in the Shanxi Formation because of higher Hg volume absorption.

The mesopores and macropores of the Shanxi Formation and Taiyuan Formation are determined by MICP.

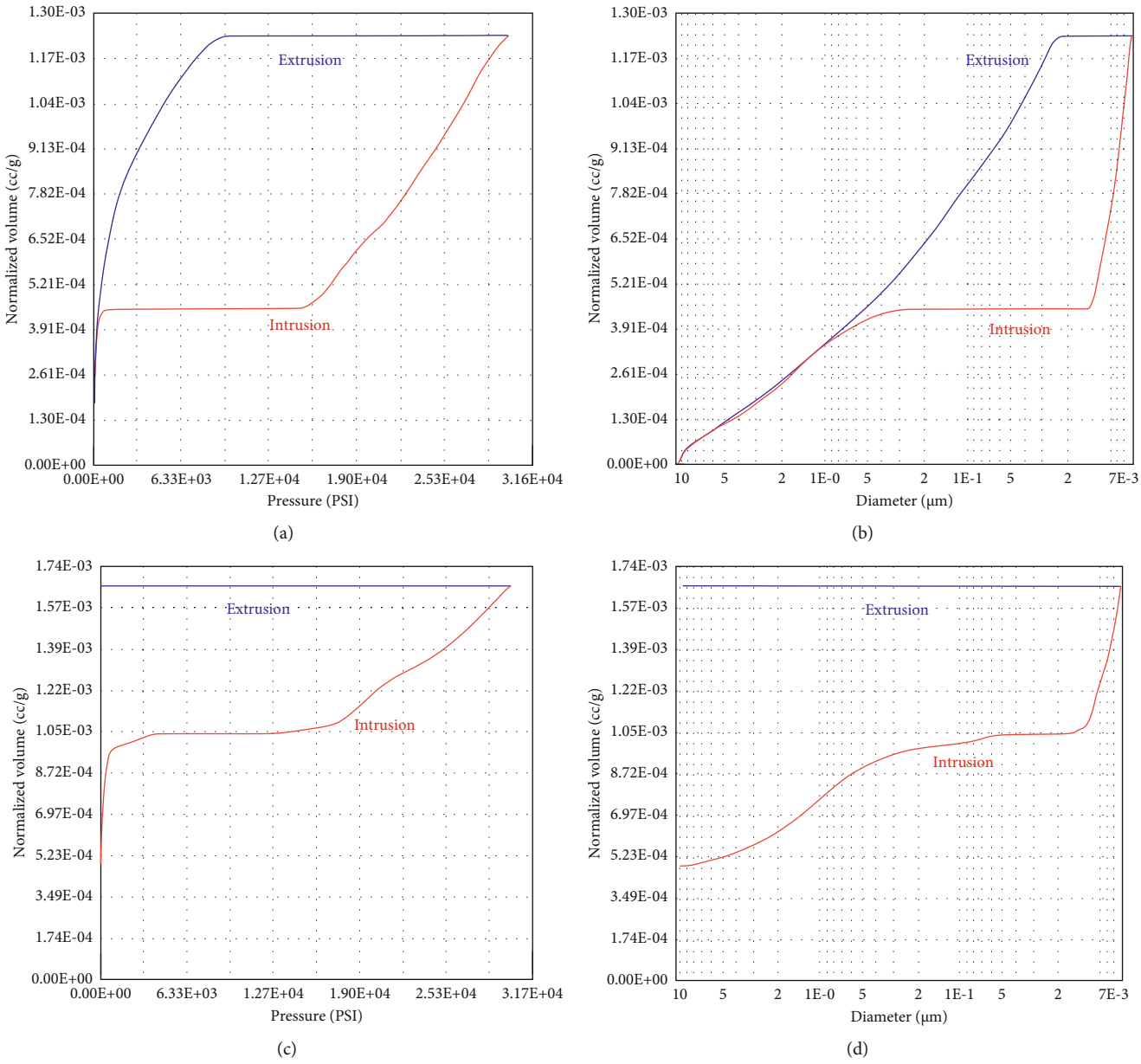

Figure 8: The intrusion and extrusion of Hg curves of the Shanxi Formation and Taiyuan Formation by MICP analysis. (a, b) Show the intrusion-extrusion MICP curves of volume with pressure and pore diameter for the Shanxi Formation. (c, d) Show the intrusion-extrusion MICP curves of volume with pressure and pore diameter for the Taiyuan Formation.

The pore size distribution is plotted against the differential pore volume of mesopores and macropores. The differential pore volume curves versus pore diameters of the mesopores and macropores of the Shanxi Formation and Taiyuan Formation are shown in Figures 9(a) and 9(b). The PSD parameters of the Shanxi Formation derived from the MICP range from 8 nm (mesopores) to 10,000 nm (macropores) (Figure 9(a)). The PSD parameters of the Taiyuan Formation resulting from the MICP extend from 7 nm to 10,000 nm (mesopores to macropores, respectively) (Figure 9(b)). The analysis of this data shows that both types of shales have similar PSD of mesopores and macropores in the Shanxi Formation and Taiyuan Formation. The mesopores in both types of shales contribute to the significant pore volume while macropores' contributions are lower than mesopores' contributions to the pore volume. These results show that the Shanxi Formation and Taiyuan Formation have abundant mesopore distribution initially, and then many of these pores were converted into macropores due to some structural deformation after diagenetic events. These structural deformations might transform the mesopores of the Shanxi Formation and Taiyuan Formation into macropores. This phenomenon might play a significant role in enhancing the pore connectivity caused by nanoscale cracking.

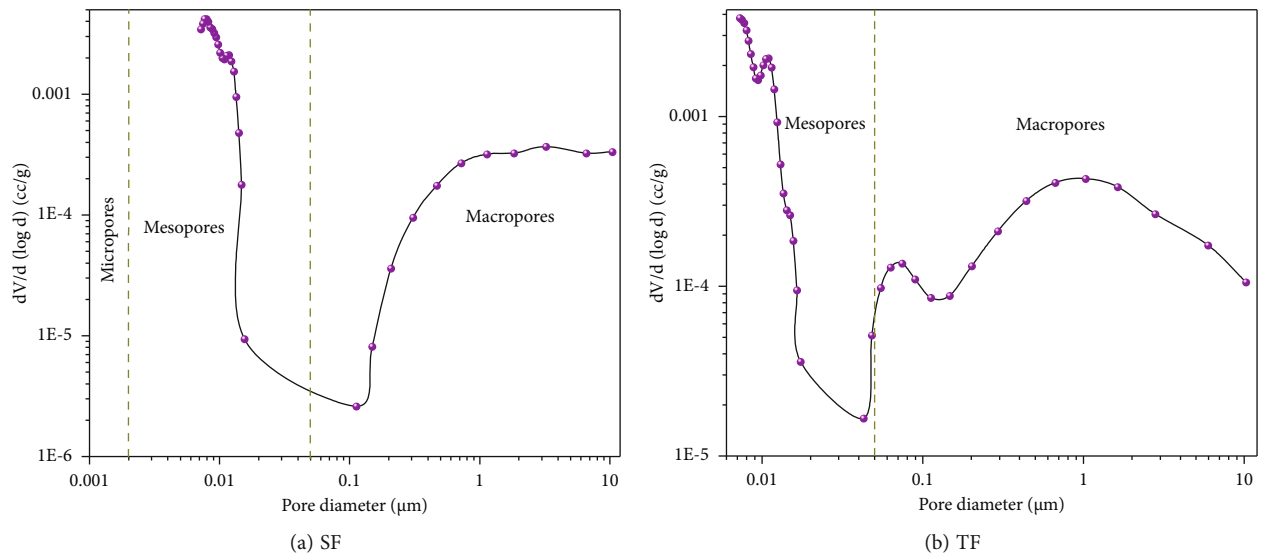

Figure 9: Showing the distribution of mesopores and macropores in the Shanxi Formation and Taiyuan Formation. (a) Distribution of mesopores and macropores in the Shanxi Formation. (b) Distribution of mesopores and macropores in the Taiyuan Formation.

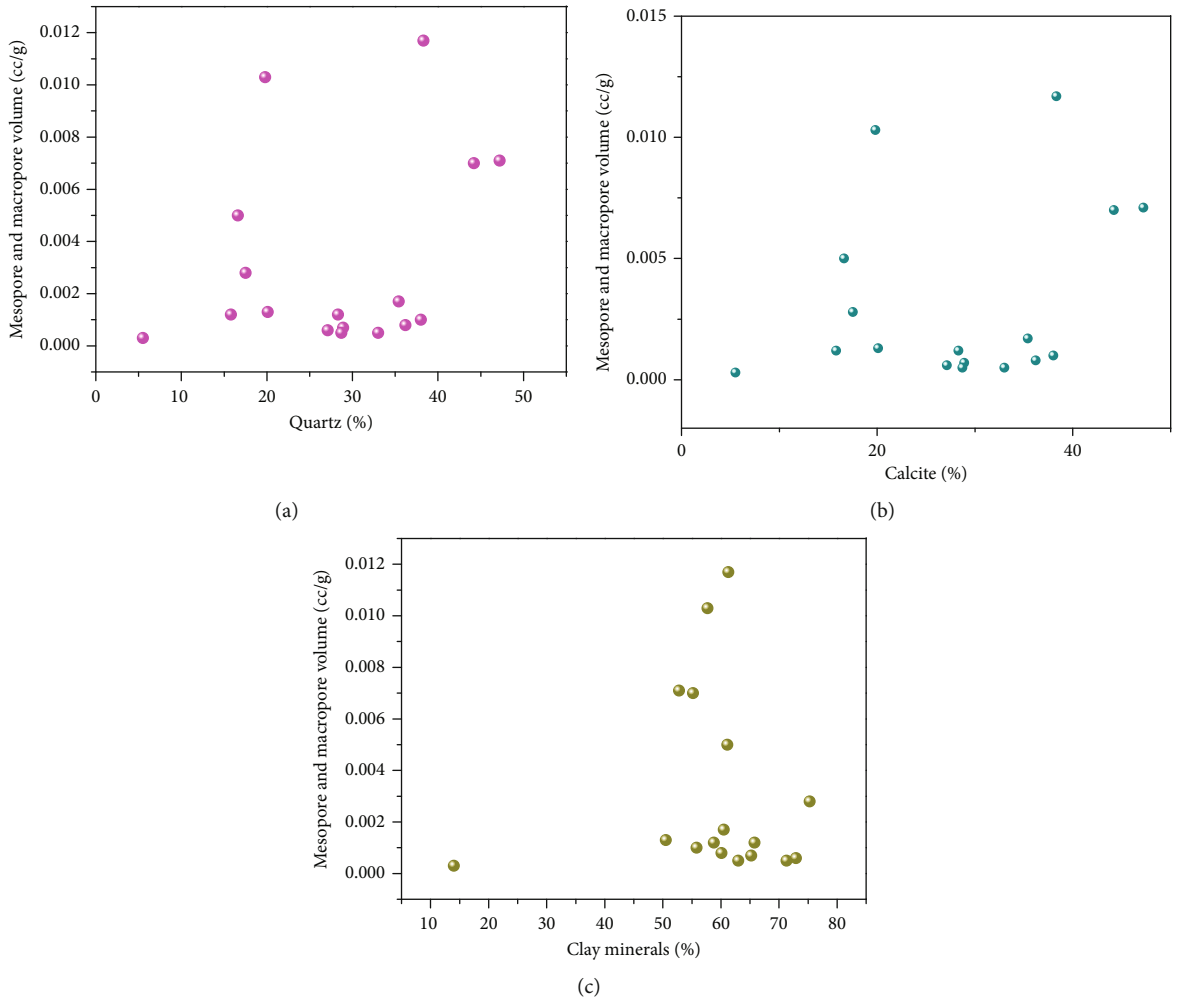

Figure 10: Shows the plot correlations between meso-macropore volume versus different minerals in the Shanxi Formation and Taiyuan Formation: (a) plot correlation between meso-macropore volume versus quartz, (b) plot correlation between meso-macropore volume versus calcite, and (c) plot correlation between meso-macropore volume versus clay minerals in the Shanxi Formation and Taiyuan Formation.

Table 3: Methane gas sorption capacity of the shale samples at 70°C from the Lower Permian Shanxi Formation and Taiyuan Formation in the Ordos Basin. Note: V_L and P_L are the Langmuir volume and pressure at which the sorbed methane gas volume reached half of P_L. R^2 = correlation coefficient; D.A.F = dry ash-free.

Formation	Depth (m)	P_L (kPa) as received	V_L (m^3/t) as received	P_L D.A.F	V_L D.A.F	R^2
Shanxi	2144.99	2630.4	5.391	2630.4	21.783	0.9994
	2145.29	2613.9	3.096	2613.9	15.844	0.9994
	2145.43	2737	5.178	2737	21.24	0.9994
	2145.68	2724	6.392	2724	17.262	0.9992
	2146.07	2516.2	4.085	2516.2	15.772	0.9995
	2146.31	1929.2	9.913	1929.2	21.659	0.9995
	2146.925	2308.7	13.792	2308.7	26.812	0.9996
	2147.205	1889.9	6.528	1889.9	18.546	0.999
	2163.58	4564.5	0.915	4564.5	9.977	0.9966
Taiyuan	2164.585	11958.2	0.994	11958.2	2.322	0.9931
	2165.25	1130.7	0.47	1130.7	1.133	0.9998
	2165.41	2555.5	24.55	2555.5	29.391	0.9998
	2165.67	2278.7	2.539	2278.7	14.163	0.9994
	2166.005	2872.1	3.74	2872.1	18.553	0.9995
	2166.725	5791.1	6.771	2791.1	35.823	0.9922
	2167.09	5392.7	5.576	5392.7	30.388	0.9941
	2167.455	5799.9	6.566	5799.9	32.96	0.9935
	2167.69	4733.1	4.883	4733.1	26.758	0.9986

The correlation plots between the different minerals and the pore volumes of the meso-macropores are revealed in plot diagrams. The correlation plot between quartz versus pore volume of the meso-macropores of the Shanxi Formation and Taiyuan Formation is weakly positive (Figure 10(a)), and this relation suggests that the quartz mineral has a very low contribution to the meso-macropore volume. The correlation between calcite versus pore volume of the meso-macropores shows a very weak negative relationship (Figure 10(b)), suggesting that the calcite has no contribution to the meso-macropore volume. The clay minerals show no correlation with the pore volume of the meso-macropores (Figure 10(c)), which shows that clay minerals also did not play a good role in meso-macropore volume contribution. Overall, minerals did not show a strong contribution to the meso-macropore volume. So, here, we can also propose that the diagenetic events and TOC can have a good contribution to the meso-macropore volume, but it needs further analysis regarding TOC to confirm this hypothesis.

4.2.4. High-Pressure Methane Adsorption Technique. The methane gas sorption capacity at 70°C for all the representative samples of the Shanxi Formation and Taiyuan Formation is displayed in Table 3. The methane gas sorption volume of the Shanxi Formation samples ranges from 0.915 to 13.792 m^3/t (for received samples) while from 9.977 to 26.812 m^3/t (for dry ash-free samples) at 1889-4564.5 kPa/70°C. The methane sorption volume of the Taiyuan Formation samples ranges from 0.47 to 24.55 m^3/t (for received samples) while from 1.133 to 35.823 m^3/t (for dry ash-free samples) at 1130.7-11958.2 kPa/70°C. The results show that the samples of the Taiyuan Formation exhibit the highest methane gas sorption volume in both samples (received samples and dry ash-free samples) while the Shanxi Formation has the lowest gas sorption capacity.

Methane sorption is known as a physical sorption process, especially in a porous shale reservoir, which is related to the van der Waals force between the asymmetrical gas surface and the gas molecules and the contact between the gas molecules [52, 53]. This thermodynamic process for methane gas sorption in shale generally recognized that the effects of temperature and pressure on the sorption capacity of methane in shale are complex [20, 54, 55]. This deduction is confirmed by our research in this study. Methane gas sorption capacity of SF and TF shale samples at 70°C increases gradually with pressure ranging from 0 to 20,000 kPa (Figures 11(a) and 11(c)) and reaches its maximum sorption capacity at 25,000 kPa pressure, suggesting that the gas sorption capacity increases with increasing pressure. Due to this fact, the correlation between pressure and pressure/volume is strongly positive for both types of shales, i.e., 0.9994 and 0.9995 for SF and TF, respectively (Figures 11(b) and 11(d)).

According to the previous literature, the mineralogical composition can also affect the adsorption capacity of methane gas [56]; this shows that the shale minerals have significant surface areas that can absorb a certain amount of methane gas [17, 57, 58]. XRD results show that the SF and TF are composed of a higher amount of quartz, calcite,

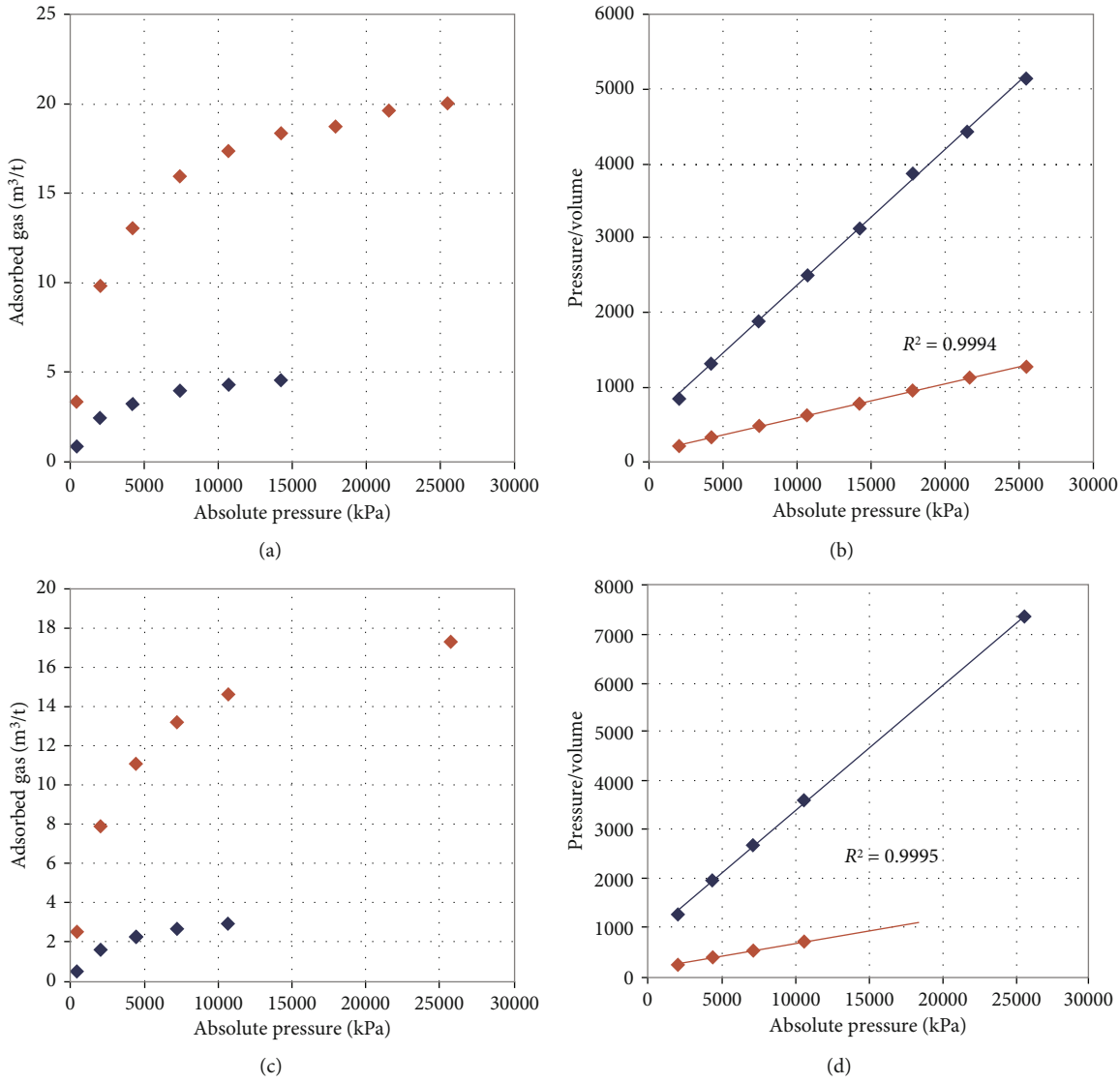

Figure 11: (a, b) Shows the methane adsorption capacity with high pressure in the SF, 2144.99 m. (c, d) Shows the methane adsorption capacity with high pressure in the TF, 2166.005 m.

and clay minerals. The plots of Langmuir sorption volume of the dry ash-free samples versus quartz, calcite, and clay minerals are shown in Figures 12(a)–12(c), respectively. Quartz shows a weak positive relation and calcite shows a negative relation with Langmuir sorption volume, but clay minerals show a strong positive correlation with Langmuir sorption volume. These correlations show that the quartz and clay minerals (R^2 of 0.23 and 0.45, respectively) in our study area have larger methane sorption capacity than calcite and other smaller amount minerals. These results are the same as the previous studies on the Paleozoic shale and Mesozoic shale in Netherland [17] and Devonian shale in the US [59], where methane sorption volume increases with clay mineral contents. But it is considered irrelevant to the sorption capacity of methane because of its nonadsorptive behavior in those shales [16, 24], but this statement is quite contradictive with our results because in our analysis, the correlation between quartz and Langmuir volume shows that the quartz also plays an important role, contributing to a certain amount of adsorption sites for methane sorption.

4.3. The Porosity of the Shanxi Formation and Taiyuan Formation by MICP. The average total porosities of the Shanxi Formation and Taiyuan Formation measured by MICP analysis are 1.52% and 0.25%, respectively. The InterP and IntraP pores contribute to the total porosity of the Shanxi Formation and Taiyuan Formation. The average InterP and IntraP porosities of the Shanxi Formation are 0.074% and 1.45%, respectively, with total porosity of 1.52%, while the average InterP and IntraP porosities of the Taiyuan Formation are 0.039% and 0.211%, respectively, with total porosity of 0.251% (Table 4). So, from the above results, we can suggest that the total porosity of the SF is higher than that of the TF.

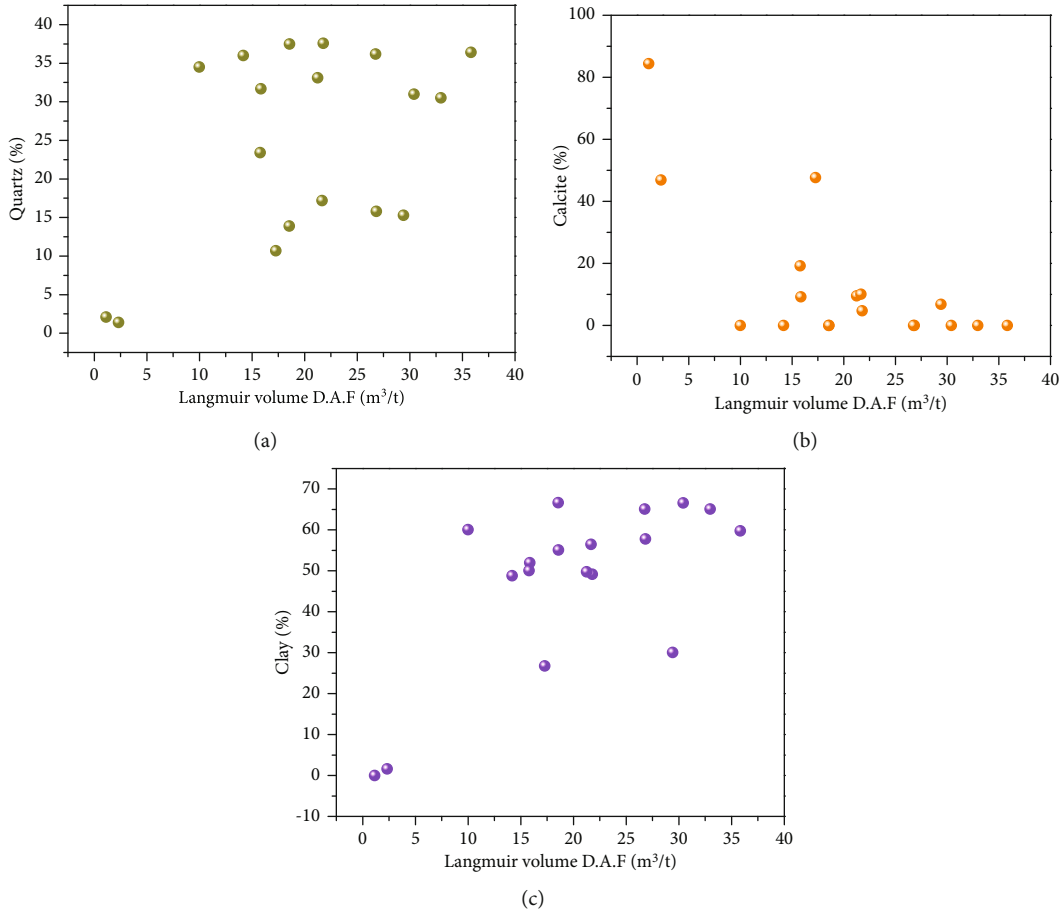

Figure 12: (a) Shows the plot correlation between Langmuir volume of dry ash-free samples versus quartz. (b) Shows the plot correlation between Langmuir volume of dry ash-free samples versus calcite. (c) Shows the plot correlation between Langmuir volume of dry ash-free samples versus clay minerals.

Table 4: Distribution of InterP porosity, IntraP porosity, and total porosity of the SF and TF in the Ordos Basin.

Formation	Depth (m)	InterP porosity (%)	IntraP porosity (%)	Total porosity (%)
Shanxi	2145.86	0.0382	0.2723	0.3105
	2146.23	0.0452	0.2670	0.3122
	2146.48	0.0124	1.2231	1.2354
	2147.11	0.0960	2.4196	2.5156
	2147.49	0.1028	1.6138	1.7167
	2147.9	0.1473	2.6936	2.8408
	2148.28	0.0824	1.6788	1.7612
Taiyuan	2164.31	0.0350	0.0461	0.0812
	2165.61	0.0298	0.6625	0.6923
	2165.87	0.0547	0.1832	0.2379
	2166.09	0.0028	0.1692	0.172
	2166.95	0.0215	0.0972	0.1188
	2167.23	0.0438	0.2645	0.3083
	2167.69	0.0461	0.1591	0.2052
	2168.04	0.1333	0.2807	0.414
	2168.26	0.0290	0.1184	0.1474
	2168.41	0.0000	0.1377	0.1377

5. Conclusions

The reservoir properties of the Shanxi Formation and Taiyuan Formation are studied in detail in this research work. Several advanced methodologies have been employed to investigate the pore properties of the Shanxi Formation and Taiyuan Formation in the Ordos Basin. After detailed analytical experiments, the following conclusions have been drawn:

(1) The dominant mineral composition of the Shanxi Formation (SF) is composed of quartz (average of 38.4%), plagioclase (average of 2.24%), siderite (average of 3.70%), Fe-dolomite (average of 3%), calcite (average of 1%), pyrite (average of 1.29%), and clay minerals (average of 50.1%), while the Taiyuan Formation (TF) is composed of calcite (average of 37%), siderite (average of 1.24%), Fe-dolomite (average of 3.69%), quartz (average of 21.9%), pyrite (average of 1.59%), and clay minerals (average of 32.3%)

(2) Micropores are abundantly distributed in these formations. The micropore surface area of the TF is higher than that of the SF. The mineral contents did not show a good relationship with the DFT

volume of micropores, suggesting that OM plays an important in the DFT pore volume of the micropores

(3) Mesopores and macropores are also lavishly scattered in these two formations. SF and TF have similar PSD of mesopores and macropores in the Ordos Basin. The mesopores contribute to the significant pore volume while macropores' contributions are lower than mesopores' contributions to the pore volume. The mineral contents did not show a good relationship with the meso-macropore volume

(4) The capacity of methane adsorption increases with increasing pressure. Clay minerals and quartz played an important role in providing adsorption sites for methane gas

(5) The average InterP and IntraP porosities of the SF are 0.074% and 1.452%, respectively, with total porosity of 1.527%, while the average InterP and IntraP porosities of the TF are 0.039% and 0.211%, respectively, with total porosity of 0.251%

(6) All the above parameters confirm that the TF has favorable reservoir properties than SF

Data Availability

Data are available upon request to the corresponding author's email address: 137910299@qq.com.

Conflicts of Interest

The authors declare that they have no conflicts of interest.

References

[1] A. C. Scott and I. J. Glasspool, "Charcoal reflectance as a proxy for the emplacement temperature of pyroclastic flow deposits," *Geology*, vol. 33, no. 7, pp. 589–592, 2005.

[2] D. W. Zhang, "Strategic concepts of accelerating thesurvey, exploration and exploitation of shale gas resourcesin China (in Chinese)," *Oil & Gas Geology*, vol. 31, pp. 135–150, 2010.

[3] X. Zhang, W. Shi, Q. Xu et al., "Reservoir characteristics and controlling factors of shalegas in Jiaoshiba area, Sichuan Basin," *Acta Petrologica Sinica*, vol. 36, pp. 926–939, 2015.

[4] C. N. Zou, D. Z. Dong, S. J. Wang et al., "Geological characteristics and resource potential of shale gas in China," *Petroleum Exploration and Development*, vol. 37, no. 6, pp. 641–653, 2010.

[5] J. Huang, C. Zou, J. Li et al., "Shale gas generation and potential of the Lower Cambrian Qiongzhusi Formation in the Southern Sichuan Basin, China," *Petroleum Exploration and Development*, vol. 39, no. 1, pp. 75–81, 2012.

[6] C. Z. Jia, C. N. Zou, J. Z. Li, D. H. Li, and M. Zheng, "Assessment criteria, main types, basic features and resourceprospects of tight oil in China (in Chinese)," *Acta PetroleiSinica*, vol. 33, pp. 343–351, 2012.

[7] J. Zhao, R. Wang, and C. Er, "Adsorption characteristics of Chang 7shale from the Triassic Yanchang Formation in Ordos Basin, andits controlling factor," *Earth Science Frontiers*, vol. 23, pp. 146–153, 2016.

[8] H. Pang, X. Q. Pang, L. Dong, and X. Zhao, "Factors impacting on oil retention in lacustrine shale: Permian Lucaogou Formation in Jimusaer Depression, Junggar Basin," *Journal of Petroleum Science and Engineering*, vol. 163, pp. 79–90, 2018.

[9] T. J. Algeo, L. Schwark, and J. C. Hower, "High-resolution geochemistry and sequence stratigraphy of the Hushpuckney Shale (Swope Formation, eastern Kansas): implications for climato- environmental dynamics of the Late Pennsylvanian Midcontinent Seaway," *Chemical Geology*, vol. 206, no. 3-4, pp. 259–288, 2004.

[10] P. Singh, "Lithofacies and sequences stratigraphic framework of the Barnett Shale, Northeast Texas, [Ph. D. thises]," The University of Oklahoma-America, 2008.

[11] T. J. Challands, H. A. Armstrong, D. P. Maloney, J. R. Davies, D. Wilson, and A. W. Owen, "Organic-carbon deposition and coastal upwelling at mid-latitude duringthe Upper Ordovician (Late Katian): a case study from the Welsh Basin, UK," *Palaeogeography, Palaeoclimatology, Palaeoecology*, vol. 273, pp. 395–410, 2009.

[12] K. M. Hulsey, "Lithofacies characterization and sequence stratigraphic framework of some gas-bearing shales within the Horn River Basin and Cordova Embayment, [M.S. thesis]," The University of Oklahoma-America, 2011.

[13] U. Hammes and G. Frebourg, "Haynesville and Bossier mudrocks: a facies and sequence stratigraphic investigation, East Texas and Louisiana, USA," *Marine and Petroleum Geology*, vol. 31, no. 1, pp. 8–26, 2012.

[14] R. M. Slatt and N. D. Rodriguez, "Comparative sequence stratigraphy and organic geochemistry of gas shales: commonality or coincidence?," *Journal of Natural Gas Science and Engineering*, vol. 8, pp. 68–84, 2012.

[15] J. B. Curtis, "Fractured shale-gas systems," *AAPG Bulletin*, vol. 86, pp. 1921–1938, 2002.

[16] D. J. Ross and R. M. Bustin, "Shale gas potential of the Lower Jurassic Gordondale Member, northeastern British Columbia, Canada," *Bulletin of Canadian Petroleum Geology*, vol. 55, no. 1, pp. 51–75, 2007.

[17] J. Li, S. Lu, P. Zhang et al., "Estimation of gas-in-place content in coal and shale reservoirs: a process analysis method and its preliminary application," *Fuel*, vol. 259, article 116266, 2020.

[18] M. Gasparik, P. Bertier, Y. Gensterblum, A. Ghanizadeh, B. M. Krooss, and R. Littke, "Geological controls on the methane storage capacity in organic-rich shales," *International Journal of Coal Geology*, vol. 123, pp. 34–51, 2014.

[19] T. Zhang, G. S. Ellis, S. C. Ruppel, K. Milliken, and R. Yang, "Effect of organic-matter type and thermal maturity on methane adsorption in shale-gas systems," *Organic Geochemistry*, vol. 47, pp. 120–131, 2012.

[20] F. Hao, H. Zou, and Y. Lu, "Mechanisms of shale gas storage: implications for shale gas exploration in China," *AAPG Bulletin*, vol. 97, no. 8, pp. 1325–1346, 2013.

[21] T. F. Rexer, M. J. Benham, A. C. Aplin, and K. M. Thomas, "Methane adsorption on shale under simulated geological temperature and pressure conditions," *Energy & Fuels*, vol. 27, no. 6, pp. 3099–3109, 2013.

[22] G. R. L. Chalmers, R. M. Bustin, and I. M. Power, "Characterization of gas shale poresystems by porosimetry, pycnometry, surface area, and field emission scanningelectronmicroscopy/ transmissionelectron microscopy image analyses:

examplesfrom the Barnett, Woodford, Haynesville, Marcellus, and Doig units," *AAPG Bulletin*, vol. 96, no. 6, pp. 1099–1119, 2012.

[23] R. G. Loucks, R. M. Reed, S. C. Ruppel, and U. Hammes, "Spectrum of pore types and networks in mudrocks and a descriptive classification for matrix-related mudrock pores," *AAPG Bulletin*, vol. 96, no. 6, pp. 1071–1098, 2012.

[24] R. G. Loucks and S. C. Ruppel, "Mississippian Barnett Shale: lithofacies and depositional setting of a deep-water shale-gas succession in the Fort Worth Basin, Texas," *AAPG Bulletin*, vol. 91, no. 4, pp. 579–601, 2007.

[25] S. J. Wang, D. H. Li, J. Z. Li, D. Z. Dong, W. Z. Zhang, and J. Ma, "Explorationpotential of shale gas in the Ordos Basin," *Natural Gas Industry*, vol. 31, pp. 40–46, 2011.

[26] D. Y. Yan, W. H. Huang, A. Li, H. Liu, and H. L. Liu, "Preliminary analysis ofmarine-continental transitional shale gas accumulation conditions andfavorable areas in the Upper Paleozoic Ordos basin," *Journal of Northeast Petroleum University*, vol. 37, no. 5, pp. 1–9, 2013.

[27] L. M. Ye, T. J. Qi, and H. Y. Peng, "Depositional environment analysis of ShanxiFormation in eastern Ordos Basin," *Acta Sedimentologica Sinica*, vol. 26, no. 2, pp. 202–210, 2008.

[28] L. C. Kuang, D. Z. Dong, W. Y. He et al., "Geological characteristics of paralic shale gas and its exploration anddevelopment prospects in the east margin of Ordos basin, NW China," *Petroleum Exploration and Development*, vol. 47, no. 3, pp. 471–482, 2020.

[29] Y. Qi, Y. W. Ju, J. Q. Tan et al., "Organic matter provenance and depositional environment of marine-to- continental mudstones and coals in eastern Ordos Basin, China–evidence from molecular geochemistry and petrology," *International Journal of Coal Geology*, vol. 217, article 103345, 2020.

[30] S. A. Holditch, "Tight gas sands," *Journal of Petroleum Technology*, vol. 58, no. 6, pp. 86–93, 2006.

[31] M. Schmitt, C. P. Fernandes, F. G. Wolf, J. A. Bellini da Cunha Neto, C. P. Rahner, and V. S. Santiago dos Santos, "Characterization of Brazilian tight gas sandstones relating permeability and angstrom-to micron-scale pore structures," *Journal of Natural Gas Science and Engineering*, vol. 27, pp. 785–807, 2015.

[32] J. Wu, C. Liang, R. C. Yang, and J. Xie, "The significance of organic matter-mineral associations in different lithofacies in the Wufeng and Longmaxi shale-gas reservoirs in the Sichuan Basin," *Marine and Petroleum Geology*, vol. 126, article 104866, 2021.

[33] J. Lai, G. W. Wang, Y. Ran, and Z. L. Zhou, "Predictive distribution of high-quality reservoirs of tight gas sandstones by linking diagenesis to depositional facies: evidence from Xu-2 sandstones in the Penglai area of the central Sichuan basin, China," *Journal of Natural Gas Science and Engineering*, vol. 23, pp. 97–111, 2015.

[34] C. L. Lan, J. F. Zhang, W. X. Tao, Y. Z. Zhang, M. H. Yang, and J. X. Wang, "Sedimentarycharacteristics and evolution of the Upper Carboniferous Taiyuan Formation, Shenmu gasfield, northeastern Ordos basin," *Acta Geologica Sinica*, vol. 85, no. 4, pp. 533–542, 2011.

[35] X. L. Meng, H. B. Zhang, Z. J. Liu, Q. H. Feng, H. Wang, and X. M. Wang, "Dominantfactors of the low-efficiency development of the gas reservoir in Taiyuan Formationin Shenmu gasfield," *Xi'an Shiyou Daxue Xuebao(Ziran Kexue Ban)- Journal of Xi'an Shiyou University(Natural Science Edition)*, vol. 27, no. 1, p. 7e10, 2012.

[36] W. Ding, D. Zhu, J. Cai, M. Gong, and F. Chen, "Analysis of the developmental characteristics and major regulating factors of fractures in marine-continental transitional shale-gas reservoirs: a case study of the Carboniferous-Permian strata in the southeastern Ordos Basin, central China," *Marine and Petroleum Geology*, vol. 45, pp. 121–133, 2013.

[37] B. D. Ritts, A. D. Hanson, B. J. Darby, L. Nanson, and A. Berry, "Sedimentary record of Triassic intraplate extension in North China: evidence from the nonmarine NW Ordos basin, Helan Shan and Zhuozi Shan," *Tectonophysics*, vol. 386, no. 3-4, pp. 177–202, 2004.

[38] S. Dai, D. Ren, C. L. Chou, S. Li, and Y. Jiang, "Mineralogy and geochemistry of the No. 6 Coal (Pennsylvanian) in the Junger Coalfield, Ordos Basin, China," *International Journal of Coal Geology*, vol. 66, no. 4, pp. 253–270, 2006.

[39] Q. H. Xu, W. Z. Shi, X. Y. Xie et al., "Inversion and propagation of the Late Paleozoic Porjianghaizi fault (North Ordos Basin, China): controls on sedimentation and gas accumulations," *Marine and Petroleum Geology*, vol. 91, pp. 706–722, 2018.

[40] X. Tang, J. Zhang, X. Wang et al., "Shale characteristics in the southeastern Ordos Basin, China: implications for hydrocarbon accumulation conditions and the potential of continental shales," *International Journal of Coal Geology*, vol. 128-129, pp. 32–46, 2014.

[41] Y. T. Yang, W. Li, and L. Ma, "Tectonic and stratigraphic controls of hydrocarbon systems in the Ordos Basin: a multicycle cratonic basin in central China," *AAPG Bulletin*, vol. 89, no. 2, pp. 255–269, 2005.

[42] L. Ji, K. Yan, F. Meng, and M. Zhao, "The oleaginous _Botryococcus_ from the Triassic Yanchang Formation in Ordos Basin, Northwestern China: morphology and its paleoenvironmental significance," *Journal of Asian Earth Sciences*, vol. 38, no. 5, pp. 175–185, 2010.

[43] Y. H. Chen, Y. B. Wang, M. Q. Guo et al., "Differential enrichment mechanism of organic matters in the marine-continental transitional shale in northeastern Ordos Basin, China: control of sedimentary environments," *Journal of Natural Gas Science and Engineering*, vol. 83, article 103625, 2020.

[44] Y. H. Guo, H. J. Liu, B. Quan, Z. C. Wang, and K. Qian, "Upper Paleozoicsedimentary system and paleogeographic evolution of Ordos area," *Acta Sedimentologica Sinica*, vol. 16, no. 3, pp. 44–52, 1998.

[45] Y. F. Li, T. W. Zhang, G. S. Ellis, and D. Y. Shao, "Depositional environment and organic matter accumulation of Upper Ordovician- Lower Silurian marine shale in the Upper Yangtze Platform, South China," *Palaeogeography Palaeoclimatology Palaeoecology*, vol. 466, pp. 252–264, 2017.

[46] L. Zhang, D. Dong, Z. Qiu et al., "Sedimentology and geochemistry of Carboniferous-Permian marine-continental transitional shales in the eastern Ordos Basin, North China," *Palaeogeography, Palaeoclimatology, Palaeoecology*, vol. 571, article 110389, 2021.

[47] A. V. Neimark, Y. Lin, P. I. Ravikovitch, and M. Thommes, "Quenched solid density functional theory and pore size analysis of micro- mesoporous carbons," *Carbon*, vol. 47, no. 7, pp. 1617–1628, 2009.

[48] K. S. Sing, D. H. Everett, R. A. W. Haul et al., "Reporting physisorption data for gas/solid systems with special reference to the determination of surface area and porosity (Recommendations 1984)," *Pure and Applied Chemistry*, vol. 57, no. 4, pp. 603–619, 1985.

[49] J. M. Kate and C. S. Gokhale, "A simple method to estimate complete pore size distribution of rocks," *Engineering Geology*, vol. 84, no. 1-2, pp. 48–69, 2006.

[50] W. Ji, Y. Song, Z. Jiang, X. Wang, Y. Bai, and J. Xing, "Geological controls and estimation algorithms of lacustrine shale gas adsorption capacity: a case study of the Triassic strata in the southeastern Ordos Basin, China," *International Journal of Coal Geology*, vol. 134-135, pp. 61–73, 2014.

[51] I. Langmuir, "The adsorption of gases on plane surfaces of glass, mica and platinum," *Journal of the American Chemical Society*, vol. 40, no. 9, pp. 1361–1403, 1918.

[52] D. M. Ruthven, *Principles of Adsorption and Adsorption Processes*, John Wiley& Sons, New York, 1984.

[53] G. Yue, Z. Wang, X. Tang, H. Li, and C. Xie, "Physical simulation of temperature influence on methane sorption and kinetics in coal (II): temperature evolvement during methane adsorption in coal measurement and modeling," *Energy & Fuels*, vol. 29, no. 10, pp. 6355–6362, 2015.

[54] A. M. Bustin and R. M. Bustin, "Coal reservoir saturation: impact of temperature and pressure," *AAPG Bulletin*, vol. 92, no. 1, pp. 77–86, 2008.

[55] J. Tan, P. Weniger, B. Krooss et al., "Shale gas potential of the major marine shale formations in the Upper Yangtze Platform, South China, Part II: methane sorption capacity," *Fuel*, vol. 129, pp. 204–218, 2014.

[56] P. J. Crosdale, B. B. Beamish, and M. Valix, "Coalbed methane sorption related tocoal composition," *International Journal of Coal Geology*, vol. 35, pp. 147–158, 1998.

[57] L. Ji, T. Zhang, K. L. Milliken, J. Qu, and X. Zhang, "Experimental investigation of main controls to methane adsorption in clay-rich rocks," *Applied Geochemistry*, vol. 27, no. 12, pp. 2533–2545, 2012.

[58] T. F. Rexer, E. J. Mathia, A. C. Aplin, and K. M. Thomas, "High-pressure methane adsorption and characterization of pores in Posidonia shales and isolated kerogens," *Energy & Fuels*, vol. 28, no. 5, pp. 2886–2901, 2014.

[59] D. J. K. Ross and R. Marc Bustin, "The importance of shale composition and pore structure upon gas storage potential of shale gas reservoirs," *Marine and Petroleum Geology*, vol. 26, no. 6, pp. 916–927, 2009.